The genome sequence of *T. parva* shows remarkable differences from the other apicomplexan genomes sequenced to date. It provides significant improvements in our understanding of the metabolic capabilities of *T. parva* and a foundation for studying parasite-induced host cell transformation and constitutes a critical knowledge base for a pathogen of significance to agriculture in Africa. Mining of sequence data has already proved useful in the search for candidate vaccine antigens (*3*).

References and Notes

1. R. A. I. Norval, B. D. Perry, A. S. Young, *The Epidemiology of Theileriosis in Africa* (Academic Press, London, 1992), p. 481.
2. A. A. Escalante, F. J. Ayala, *Proc. Natl. Acad. Sci. U.S.A.* **92**, 5793 (1995).
3. S. P. Graham *et al.*, in preparation.
4. A. Pain *et al.*, *Science* **309**, 131 (2005).
5. Materials and methods are available as supporting material on *Science* Online.
6. A. Kairo, A. H. Fairlamb, E. Gobright, V. Nene, *EMBO J.* **13**, 898 (1994).
7. M. J. Gardner *et al.*, *Nature* **419**, 498 (2002).
8. J. H. Gunderson *et al.*, *Science* **238**, 933 (1987).
9. B. Vogelstein, K. W. Kinzler, *Nat. Med.* **10**, 789 (2004).
10. M. Goedert, *Semin. Cell Dev. Biol.* **15**, 45 (2004).
11. I. M. Cheeseman, A. Desai, *Curr. Biol.* **14**, R70 (2004).
12. R. F. Anders, *Parasite Immunol.* **8**, 529 (1986).
13. R. Bishop *et al.*, *Mol. Biochem. Parasitol.* **110**, 359 (2000).
14. B. Sohanpal, D. Wasawo, R. Bishop, *Gene* **255**, 401 (2000).
15. H. A. Baylis, S. K. Sohal, M. Carrington, R. P. Bishop, B. A. Allsopp, *Mol. Biochem. Parasitol.* **49**, 133 (1991).
16. J. D. Barry, M. L. Ginger, P. Burton, R. McCulloch, *Int. J. Parasitol.* **33**, 29 (2003).
17. R. Bishop *et al.*, in preparation.
18. Z. Su *et al.*, *Cell* **82**, 89 (1995).
19. R. Bishop, A. Musoke, S. Morzaria, B. Sohanpal, E. Gobright, *Mol. Cell. Biol.* **17**, 1666 (1997).
20. M. S. Abrahamsen *et al.*, *Science* **304**, 441 (2004); published online 25 March 2004 (10.1126/science.1094786).
21. B. J. Foth *et al.*, *Mol. Microbiol.* **55**, 39 (2005).
22. S. A. Ralph, *Mol. Microbiol.* **55**, 1 (2005).
23. A. A. McColm, N. McHardy, *Ann. Trop. Med. Parasitol.* **78**, 345 (1984).
24. R. F. Waller, G. I. McFadden, *Curr. Issues Mol. Biol.* **7**, 57 (2005).
25. R. F. Waller *et al.*, *Proc. Natl. Acad. Sci. U.S.A.* **95**, 12352 (1998).
26. F. Seeber, *Int. J. Parasitol.* **32**, 1207 (2002).
27. X. M. Xu, S. G. Moller, *Proc. Natl. Acad. Sci. U.S.A.* **101**, 9143 (2004).
28. S. Leon, B. Touraine, C. Ribot, J. F. Briat, S. Lobreaux, *Biochem. J.* **371**, 823 (2003).
29. J. M. Carlton *et al.*, *Nature* **419**, 512 (2002).
30. R. J. Wilson *et al.*, *J. Mol. Biol.* **261**, 155 (1996).
31. Single-letter abbreviations for the amino acid residues are as follows: A, Ala; C, Cys; D, Asp; E, Glu; F, Phe; G, Gly; H, His; I, Ile; K, Lys; L, Leu; M, Met; N, Asn; P, Pro; Q, Gln; R, Arg; S, Ser; T, Thr; V, Val; W, Trp; and Y, Tyr.

32. We thank T. Irvin, O. Ole-MoiYoi, T. Musoke, C. Sugimoto, H. Leitch, R. von Kaufmann, S. MacMillan, R. Koenig, M. Brown, R. Ndegwa, L. Thairo, B. Anyona, T. Akinyemi, the TIGR conferences staff, the Secretariat of the Consultative Group for International Agricultural Research, and the research staff of the International Livestock Research Institute (ILRI). Supported by the TIGR Board of Trustees, ILRI, J. C. Venter, the Rockefeller Foundation, the U.S. Agency for International Development, and the UK Department for International Development.

Supporting Online Material

www.sciencemag.org/cgi/content/full/309/5731/134/DC1
Materials and Methods
Figs. S1 to S3
Tables S1 to S3

31 January 2005; accepted 5 May 2005
10.1126/science.1110439

Long-Term Monitoring of Bacteria Undergoing Programmed Population Control in a Microchemostat

Frederick K. Balagaddé,[1]*† Lingchong You,[2]†‡ Carl L. Hansen,[1]§ Frances H. Arnold,[2] Stephen R. Quake[1]*‖

Using an active approach to preventing biofilm formation, we implemented a microfluidic bioreactor that enables long-term culture and monitoring of extremely small populations of bacteria with single-cell resolution. We used this device to observe the dynamics of *Escherichia coli* carrying a synthetic "population control" circuit that regulates cell density through a feedback mechanism based on quorum sensing. The microfluidic bioreactor enabled long-term monitoring of unnatural behavior programmed by the synthetic circuit, which included sustained oscillations in cell density and associated morphological changes, over hundreds of hours.

By continually substituting a fraction of a bacterial culture with sterile nutrients, the chemostat (*1*, *2*) presents a near-constant environment that is ideal for controlled studies of microbes and microbial communities (*3*–*6*). The considerable challenges of maintaining and operating continuous bioreactors, including the requirement for large quantities of growth media and reagents, have pushed the move toward miniaturization and chip-based control (*7*–*10*), although efforts have been limited to batch-format operation. Microbial biofilms, which exist in virtually all nutrient-sufficient ecosystems (*11*), interfere with continuous bioreactor operation (*12*). Phenotypically distinct from their planktonic counterparts (*11*), biofilm cells shed their progeny into the bulk culture and create mixed cultures. At high dilution rates, the biofilm, which is not subject to wash-out, supplies most of the bulk-culture cells (*13*). The increase in surface area-to-volume ratio as the working volume is decreased aggravates these wall-growth effects (*13*).

We created a chip-based bioreactor that uses microfluidic plumbing networks to actively prevent biofilm formation. This device allows semicontinuous, planktonic growth in six independent 16-nanoliter reactors with no observable wall growth (Fig. 1A). The cultures can be monitored in situ by optical microscopy to provide automated, real-time, noninvasive measurement of cell density and morphology with single-cell resolution.

Each reactor, or "microchemostat," consists of a growth chamber, which is a fluidic loop 10 μm high, 140 μm wide, and 11.5 mm in circumference, with an integrated peristaltic pump and a series of micromechanical valves to add medium, remove waste, and recover cells (Fig. 1B). The growth loop is itself composed of 16 individually addressable segments. The microchemostat is operated in one of two alternating states: (i) continuous circulation, and (ii) cleaning and dilution. During continuous circulation, the peristaltic pump moves the microculture around the growth loop at a linear velocity of ~250 μm s^{-1} (Fig. 1C). During cleaning and dilution, the mixing is halted and a segment is isolated from the rest of the reactor with micromechanical valves. A lysis buffer is flushed through the isolated segment for 50 s to expel the cells it contains, including any wall-adhering cells (Fig. 1D). Next, the segment is flushed with sterile growth medium to completely rinse out the lysis buffer. This segment, filled with sterile medium, is then reunited with the rest of the growth chamber, at which point continuous circulation resumes. This process is repeated sequentially on different growth chamber segments, thus eliminating biofilm formation and enabling pseudocontinuous operation. In comparison, passive treatment of the microfluidic surfaces with nonadhesive surface coatings [such as poly (ethylene glycol), ethylenediaminetetraacetic acid, polyoxyethylene sorbitan monolaurate, and bovine serum albumin] proved ineffective in preventing biofilm forma-

[1]Department of Applied Physics, [2]Division of Chemistry and Chemical Engineering, California Institute of Technology, Pasadena, CA 91125, USA.

*Present address: Department of Bioengineering, Stanford University, Stanford, CA 94305, USA.
†These authors contributed equally to this work.
‡Present address: Department of Biomedical Engineering and Institute for Genome Sciences and Policy, Duke University, Durham, NC 27708, USA.
§Present address: Department of Physics and Astronomy, University of British Columbia, Vancouver, BC V6T 1Z4, Canada.
‖To whom correspondence should be addressed. E-mail: quake@stanford.edu

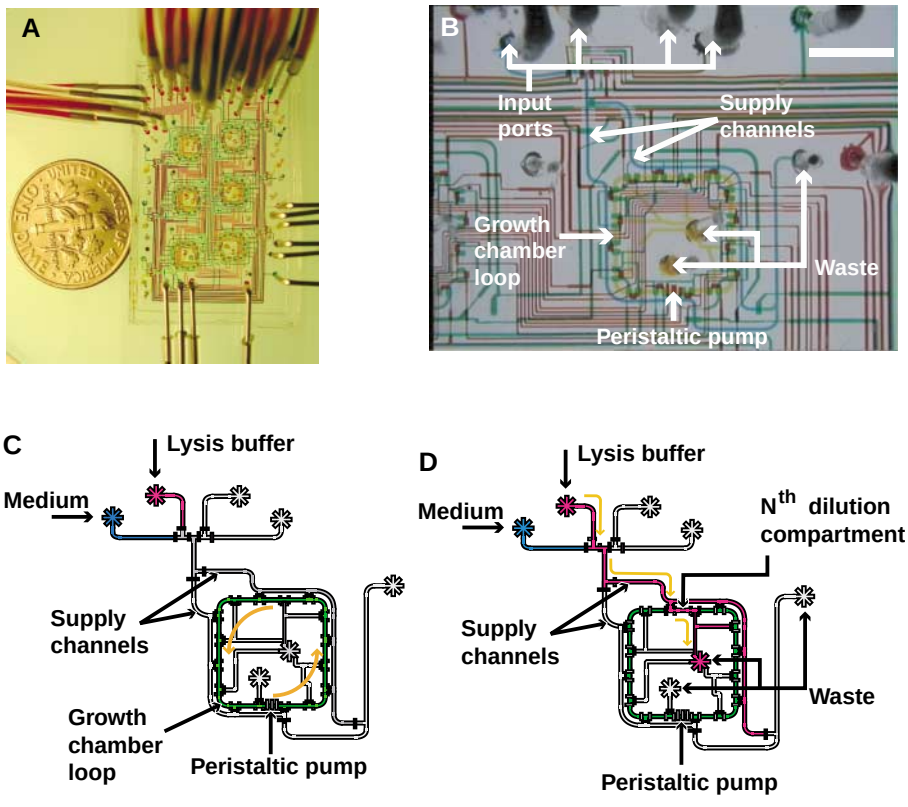

Fig. 1. (**A**) Optical micrograph showing six microchemostats that operate in parallel on a single chip. Various inputs have been loaded with food dyes to visualize channels and sub-elements of the microchemostats. The coin is 18 mm in diameter. (**B**) Optical micrograph showing a single microchemostat and its main components. Scale bar, 2 mm. (**C**) Schematic diagram of a microchemostat in continuous circulation mode. Elements such as the growth loop with individually addressable connected segments, the peristaltic pump, supply channels, and input/output ports are labeled. (**D**) Isolation of a segment from the rest of the growth chamber during cleaning and dilution mode. A lysis buffer (indicated in red) is introduced into the chip through the lysis buffer port. Integrated microvalves direct the buffer through the segment, flushing out cells, including those adhering to chamber walls. The segment is then rinsed with fresh sterile medium and reunited with the rest of the growth chamber.

tion. Without active removal, biofilms invaded the fluidic channels within ~48 hours (*14*).

We performed more than 40 growth experiments with *Escherichia coli* MG1655 cells in five different chips, using a variety of growth media ([MOPS EZ Rich (Teknova, Inc.)] and LB broth with various concentrations of glucose and bacto-tryptone) at 21°C and 32°C. Upon inoculation, a typical culture began with a short lag period, followed by an exponential growth phase that gave way to a steady-state regime (Fig. 2A). Steady-state growth was achieved over a range of dilution rates (0.072 to 0.37 $hour^{-1}$); wash-out was observed at high dilution rates. The steady-state cell concentrations scaled with dilution rate and nutrient richness, decreasing with increasing dilution rates or decreasing bacto-tryptone concentration (Fig. 2B).

To demonstrate the ability of the microchemostat to facilitate analysis of complex growth dynamics, we used it to monitor the dynamics of cell populations containing a synthetic "population control" circuit (*15*), which autonomously regulates the cell density through a negative feedback system based on quorum sensing (*16*). With the circuit ON, the cell density is broadcast and detected through the synthesis and sensing of a signaling molecule (acyl-homoserine lactone, or AHL), which in turn modulates the expression of a killer gene (*lacZα-ccdB*). The killer gene regulates cell density by controlling the cell death rate. The circuit, under control of a synthetic promoter, is inducible with isopropyl-β-D-thiogalactopyranoside (IPTG) (fig. S1). The population control circuit's use of cell-cell communication enables the programming of a bacterial population such that the circuit is insulated from noise in gene expression as

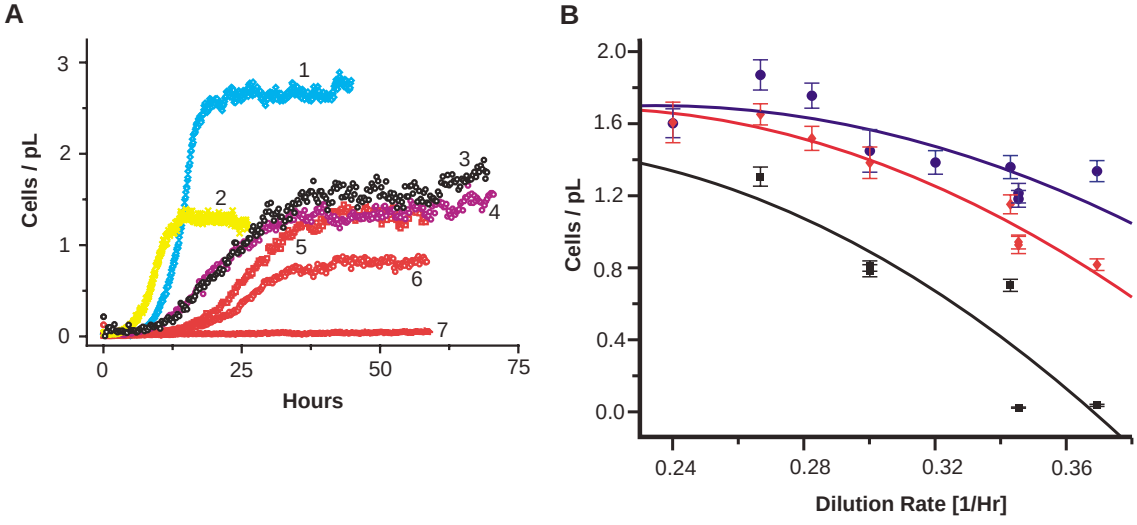

Fig. 2. (**A**) Bacterial growth as a function of time in various media and dilution rates *D*: (1) MOPS EZ Rich, in 1.1 M glucose, $D = 0.34\ hour^{-1}$, at 32°C; (2) MOPS EZ Rich, in 0.11 M glucose, $D = 0.30\ hour^{-1}$, at 32°C; (3) LB, in 0.5 g/L of bacto-tryptone, $D = 0.24\ hour^{-1}$, at 21°C; (4) LB, in 0.5 g/L of bacto-tryptone, $D = 0.30\ hour^{-1}$, at 21°C; (5) LB, in 3 g/L of bacto-tryptone, $D = 0.37\ hour^{-1}$, at 21°C; (6) LB, in 0.5 g/L of bacto-tryptone, $D = 0.37\ hour^{-1}$, at 21°C; and (7) LB, in 0.1 g/L of bacto-tryptone, $D = 0.37\ hour^{-1}$, at 21°C. The red curves (5, 6, and 7) represent different concentrations of bacto-tryptone in LB at a fixed dilution rate, and the open circles (3, 4, and 6) represent constant influent nutrient composition at various dilution rates. Cultures 3 to 7 were cultivated on a single chip, whereas cultures 1 and 2 were each cultivated on separate chips. (**B**) Graph showing steady-state populations for various choices of dilution rate and nutrient concentrations. The error bars represent the variation in the measured steady-state cell density. The steady-state concentration decreases as the dilution rate increases and increases in proportion to the influent nutrient richness. Black squares, 0.1 g/L of bacto-tryptone; red diamonds, 0.5 g/L of bacto-tryptone; blue circles, 3 g/L of bacto-tryptone.

well as intercellular phenotypical variability. This circuit has been characterized in detail for macroscopic cultures (*15*), which makes it particularly appropriate for evaluating performance of the microchemostat in a well-controlled manner.

A microchemostat chip was used to perform six simultaneous experiments with *E. coli* MC4100Z1 cells and a dilution rate of 0.16 hour^{-1} (Fig. 3A). Cultures in reactors 1 to 3 with circuit-bearing cells were induced with IPTG (circuit ON), whereas those in 5 and 6 were not induced (circuit OFF). Reactor 4 contained a circuit-free population with IPTG. Circuit-free and circuit-OFF cultures (4, 5, and 6) grew exponentially to a steady-state density of ~3.5 cells/pL. In contrast, circuit-ON populations (1, 2, and 3) exhibited oscillatory dynamics before reaching a lower steady-state population density after ~125 hours. Variations in cell density due to the discretized nature of the microchemostat dilution scheme were negligible compared to the overall population fluctuations (Fig. 3B).

Using the ability to monitor individual cells in the microchemostat cultures, we observed that the oscillations in cell density correlated with specific cell morphologies (Fig. 3A). For example, upon inoculation, culture 3 (Fig. 3A, point a) was composed of healthy (small and cylindrical) cells. With negligible expression of the killer protein (LacZα-CcdB) at such low density, the population initially enjoyed exponential growth, in tandem with the OFF cultures. The cells were generally healthy during this phase, evident in their morphology (Fig. 3A, point b). However, as the increased cell density led to increased AHL concentration and, consequently, increased expression of the killer protein (Fig. 3A, point c), the cell density began to decrease. By this time, a fraction of cells had become filamented, showing the deleterious effect of LacZα-CcdB; due to a lag in the turnover of the signal (by dilution and degradation) and that of the killer protein (by cell division and degradation), cell death intensified (Fig. 3A, point d), leading to a sharp decrease in the cell density. Further decreases in cell density ultimately led to a decrease in the signal concentration as well as the killer protein concentration. Eventually, when the death rate dropped below the growth rate as the killer protein was diluted out (Fig. 3A, point e), the population recovered and entered the next cycle. Culture 3 escaped circuit regulation after 186 hours. Under these conditions, the bacterial population oscillated for 4 to 6 cycles before approaching a steady-state concentration of ~2 cells/pL. Cultures 1 and 2 demonstrated similar dynamics.

Different cell morphologies and circuit dynamics were apparent when the population control circuit was introduced into a different *E. coli* host strain. In Top10F′ cells, more complete induction of the circuit was achieved (*14*), leading to stronger growth regulation (Fig. 4). At time 0 in these experiments (with a dilution rate of 0.16 hour^{-1}), the circuit was turned ON in cultures 1 to 3 but left OFF in cultures 4 to 6. The OFF cultures (cultures 4 to 6, 0 to 96 hours) grew to a steady-state density of ~3 cells/pL. In contrast, the ON density was sixfold lower than the OFF density and oscillated about ~0.5 cells/pL (1, 0 to 96 hours; 2 and 3, 0 to 44 hours). Top10F′ cells displayed none of the morphological responses to circuit regulation that were evident in MC4100Z1 cells; they always looked small and cylindrical, similar to circuit-OFF cells.

In general, the circuit appeared to be more stable in the microchemostats than in macroscale batch cultures under otherwise similar growth conditions. During macroscale experiments with reaction volumes of 3 to 50 ml, circuit-ON cultures lost regulation within ~70 hours for MC4100Z1 and 48 hours for Top10F′ cells (*14*). Population control in the microche-

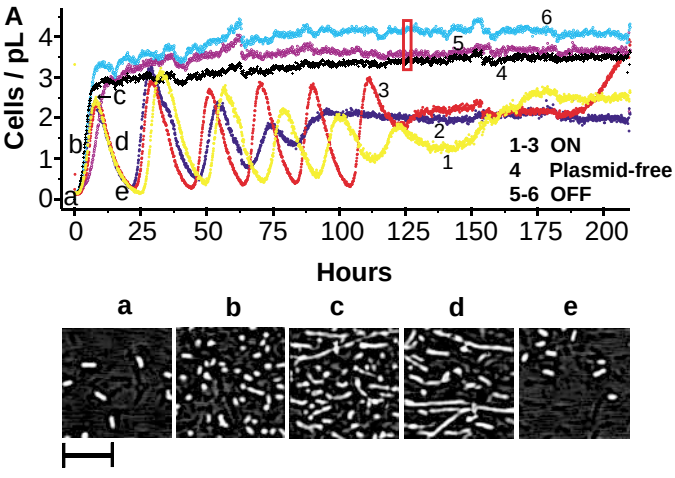

Fig. 3. (**A**) Growth of MC4100Z1 cells with the population-control circuit ON (reactors 1 to 3), OFF (reactors 5 to 6), or absent (reactor 4) on a single chip. Bottom panels (a to e) show micrographs of the culture in reactor 3 at the corresponding points during the first oscillation (scale bar, 25 μm). Cells were grown at 32°C in LBK medium (*14*), buffered at pH 7.6, at a dilution rate of 0.16 hour^{-1}. The section enclosed by the red box is enlarged in the next panel. (**B**) Zoom-in on series 4, 5, and 6, showing variation with time in cell density. The shaded strips represent dilution intermissions.

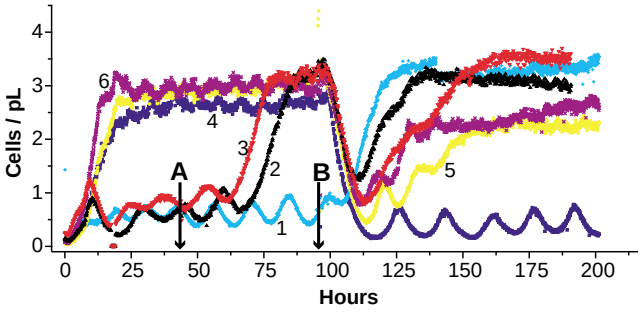

Fig. 4. Growth of Top10F′ cells with the circuit cycling between ON and OFF in the chip. Initially, cultures 1, 2, and 3 were ON, while cultures 4, 5, and 6 were OFF. At 44 hours (point A), cultures 2 and 3 were turned OFF. At 96 hours (point B), culture 1 was turned OFF, and cultures 2 to 6 were turned ON. Cultures 2 and 3 were cultivated on a separate chip in a different experiment under the same conditions. When turned OFF, culture 1 (at 96 hours) and cultures 2 and 3 (at 44 hours) grew exponentially to a density of ~3 cells/pL. Upon circuit activation at 96 hours after an extended OFF period, culture 4 generated sustained oscillations similar to those of culture 1 between 0 and 96 hours, after a rapid decrease in cell density. In comparison, when switched ON at 96 hours, cultures 2, 3, 5, and 6 only briefly demonstrated circuit regulation (evident in the sharp decrease in cell density) before bouncing back to a high density. Cells were grown at 32°C in LBK medium (*14*), buffered at pH 7.0.

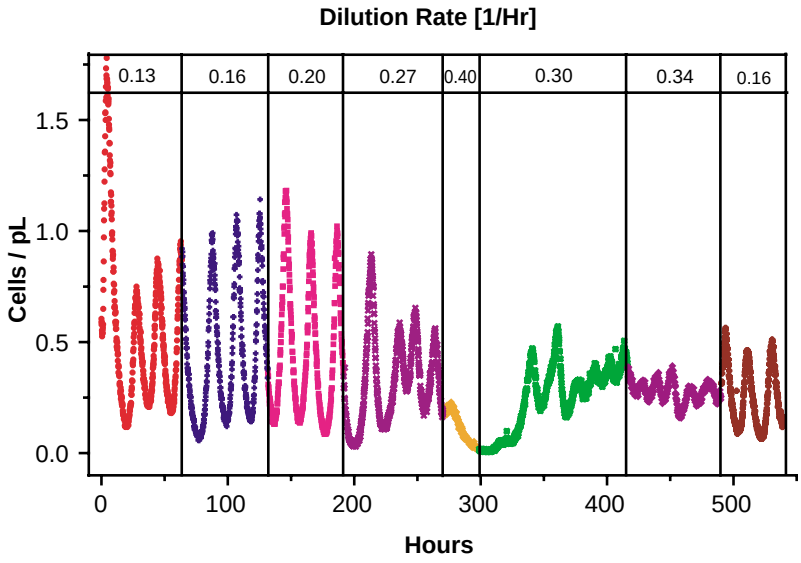

Fig. 5. Effects of the dilution rate on population dynamics of Top10F′ cells with the population-control circuit ON. At high dilution rates (to 0.27, 0.30, and 0.34 hour^{-1}), both the amplitude and the period of oscillations diminished. The culture was approaching wash-out at the highest dilution rate (0.40 hour^{-1}). Large oscillations were recovered when a low dilution rate was restored toward the end of the experiment. Cells were grown at 32°C in LBK medium (*14*), buffered at pH 7.0.

mostat, in contrast, was routinely maintained for more than 200 hours and sometimes more than 500 hours (Fig. 5). In theory, the small population size in the microchemostat (~10^2 to ~10^4 cells versus ~10^9 cells in macroscale cultures) should reduce the overall rate at which mutants may occur and take over a population. Exactly how the cells lost regulation in the circuit-ON cultures (Fig. 3, culture 3, and Fig. 4, cultures 2, 3, 5, and 6) is unclear. A simple mutation rate versus population size argument would predict much longer lifetimes for maintaining circuit regulation.

We observed oscillations in cell density for both *E. coli* strains in the circuit-ON state. The MC4100Z1 strain had large-amplitude (~2 cells/pL) oscillations, which gradually decayed to a steady state (Fig. 3A). The Top10F′ strain had smaller amplitude oscillations (~1 cell/pL) which continued for the length of the measurement (Figs. 4 and 5). Although the origin of these oscillations is unknown, they may be a consequence of the circuit interacting with the continuous culture mechanism of the microchemostat. It is also possible that the oscillations are entirely due to circuit regulation, as predicted by a simple mathematical model with biologically feasible parameters (*14*). These population-level oscillations are controllable—they only occur when the circuit is in the ON state—and they are more sustained and stable than those generated by synthetic oscillators operating in individual cells (*17*, *18*).

An active approach to preventing biofilm formation in microfluidic devices enabled us to implement a miniaturized bioreactor that operates at a working volume of 16 nL, more than 300 times smaller than the smallest previous microfermentor (*7*). This miniaturized device enabled automated culturing and monitoring of populations of ~100 to ~10^4 bacteria with instantaneous single-cell resolution. Reducing the reactor volume by a factor of 10^5 can, in theory, suppress the total mutation rate proportionately and hence prolong monitoring of genetically homogeneous populations (*14*). The microchemostat has enabled us to monitor the programmed behavior of bacterial populations for hundreds of hours despite strong selection pressure to evade population control, something that was not achieved in macroscopic reactors. Although we focused on the bacterial count and cell morphology, measurements can be readily extended to dynamic properties, for example, gene expression dynamics and distributions reported by fluorescence or luminescence. These capabilities enable long-term, low-cost, high-resolution investigation of the phenotypical characteristics of many different cell strains, as well as natural and synthetic cellular networks under a matrix of conditions. This capability will greatly facilitate high-throughput screening applications in fields such as chemical genetics and pharmaceutical discovery.

References and Notes

1. J. Monod, *Ann. Inst. Pasteur (Paris)* **79**, 390 (1950).
2. A. Novick, L. Szilard, *Science* **112**, 715 (1950).
3. D. E. Dykhuizen, *Annu. Rev. Ecol. Syst.* **21**, 373 (1990).
4. M. S. Fox, *J. Gen. Physiol.* **39**, 267 (1955).
5. H. L. Smith, P. Waltman, in *The Theory of the Chemostat: Dynamics of Microbial Competition* (Univ. of Cambridge Press, Cambridge, ed. 1, 1995).
6. A. Novick, *Annu. Rev. Microbiol.* **9**, 97 (1955).
7. A. Zanzotto *et al.*, *Biotechnol. Bioeng.* **87**, 243 (2004).
8. J. W. Kim, Y. H. Lee, *J. Korean Phys. Soc.* **33**, S462 (1998).
9. Y. Kostov, P. Harms, L. Randers-Eichhorn, G. Rao, *Biotechnol. Bioeng.* **72**, 346 (2001).
10. M. M. Maharbiz, W. J. Holtz, R. T. Howe, J. D. Keasling, *Biotechnol. Bioeng.* **85**, 376 (2004).
11. J. W. Costerton, Z. Lewandowski, D. E. Caldwell, D. R. Korber, H. M. Lappinscott, *Annu. Rev. Microbiol.* **49**, 711 (1995).
12. H. H. Topiwala, C. Hamer, *Biotechnol. Bioeng.* **13**, 919 (1971).
13. D. H. Larsen, R. L. Dimmick, *J. Bacteriol.* **88**, 1380 (1964).
14. Materials and methods are available as supporting material on *Science* Online.
15. L. You, R. S. Cox III, R. Weiss, F. H. Arnold, *Nature* **428**, 868 (2004).
16. M. B. Miller, B. L. Bassler, *Annu. Rev. Microbiol.* **55**, 165 (2001).
17. M. B. Elowitz, S. Leibler, *Nature* **403**, 335 (2000).
18. M. R. Atkinson, M. A. Savageau, J. T. Myers, A. J. Ninfa, *Cell* **113**, 597 (2003).

19. We thank M. Elowitz for MC4100Z1 cells, U. Alon for MG1655 cells, T. Ozdere for generating data for figs. S4 and S5, C. Collins for plasmid pLuxR, M. Barnett for technical assistance, and J. Leadbetter, C. Ward, T. Squires, J. Huang, and E. Kartalov for helpful discussions. Supported in part by the NSF and the Defense Advanced Research Projects Agency (contract no. N66001-02-1-8929).

Supporting Online Material
www.sciencemag.org/cgi/content/full/309/5731/137/DC1
Materials and Methods
Figs. S1 to S5
Tables S1 and S2
References and Notes

27 December 2004; accepted 10 May 2005
10.1126/science.1109173

tRNA Actively Shuttles Between the Nucleus and Cytosol in Yeast

Akira Takano,[1] Toshiya Endo,[1,3,4] Tohru Yoshihisa[1,2]*

Previous evidence suggested that transfer RNAs (tRNAs) cross the nuclear envelope to the cytosol only once after maturing in the nucleus. We now present evidence for nuclear import of tRNAs in yeast. Several export mutants accumulate mature tRNAs in the nucleus even in the absence of transcription. Import requires energy but not the Ran cycle. These results indicate that tRNAs shuttle between the nucleus and cytosol.

Nuclear-encoded tRNAs are transcribed, processed in the nucleus, and exported to the cytosol to facilitate translation (*1*). Moreover, a nuclear pool of mature tRNAs also exists. In *Saccharomyces cerevisiae*, certain mutants defective in nuclear transport and tRNA processing accumulate mature tRNAs in the nucleus, which suggests that nuclear mature tRNAs are intermediates waiting for tRNA export (*2*–*5*). Before export, aminoacyl-tRNA synthetases